Understanding the Relationship Between Structure and Thermophysical Properties of CaO-SiO$_2$-MgO-Al$_2$O$_3$ Molten Slags

YONGQI SUN, HAO WANG, and ZUOTAI ZHANG

In the present work, the relationship between the microscopic structure and macroscopic thermophysical properties in a basic CaO-SiO$_2$-MgO-Al$_2$O$_3$ quaternary system was identified using Fourier transformation infrared, Raman and ^{27}Al magic angular spinning nuclear magnetic resonance (MAS-NMR) techniques. The Raman spectra quantitatively proved that with increasing Al$_2$O$_3$ content, the concentrations of the symmetric units of Q^0(Si) and Q^2(Si) decreased, while those of the asymmetric units of Q^1(Si) and Q^3(Si) increased; consequently, the degree of polymerization of the networks increased, which resulted in an increase in slag viscosity. The ^{27}Al MAS-NMR spectra demonstrated that three structural units of Al atoms, namely, AlO$_4$, AlO$_5$, and AlO$_6$, mainly existed in the networks. With increasing Al$_2$O$_3$ content, the concentration of AlO$_4$ slightly decreased, while those of AlO$_5$ and AlO$_6$ increased; overall, Al$_2$O$_3$ acted as a network former in the present system. The increasing Al$_2$O$_3$ content led to additional AlO$_6$ and Si-NBO-Ca-NBO-Al frameworks, which replaced Si-NBO-Ca-NBO-Si in the networks (NBO: non-bridging oxygen) and induced a change in the primarily precipitated crystalline phase from Ca$_2$MgSi$_2$O$_7$ and Ca$_2$Al$_2$SiO$_7$ to MgAlO$_4$.

I. INTRODUCTION

RECENTLY, with continuous mining and consumption, the ores rich in irons are gradually diminishing, and low-degree iron ores have been increasingly used in the iron and steel sector. The degradation in iron ores results in the variation in the chemical compositions of blast furnace slags (BFSs),[1,2] and as a typical result, the Al$_2$O$_3$ content in BFSs has increased, which causes changes in the BFS macroscopic properties such as viscosity and crystallization behaviors.

Conventionally, hot BFSs at ~1823 K (1550 °C) are water quenched, and then the slags obtained in a glassy state are further utilized as raw materials in cement manufacturing.[3-5] However, using the water-quenching method, the thermal heat in hot slags has generally been wasted, and recently, various dry granulation methods such as rotary cup atomizer[6] and spinning disk atomizer[7] have been developed to recover the waste heat in slags. The main objectives of these methods are to break the liquid slags into small droplets to resist the crystallization of slags and thus facilitate transformation into a glassy state. The variation in Al$_2$O$_3$ content can change the crystallization behaviors of the BFS including crystalline phases and crystallization ability and thus change the difficulties of slag heat recovery. In previous studies,[8,9] it was found that the crystallization ability of a BFS first decreased and then increased with increasing Al$_2$O$_3$ content, as demonstrated by a varying critical cooling rate.

Generally, the macroscopic properties of slags are directly related to the microscopic structures. As an amphoteric oxide, the role of Al$_2$O$_3$ in a BFS is complicated and unclear, especially from the viewpoints of crystallization control and heat recovery from the slags; thus, the present study was motivated. Herein a basic quaternary CaO-SiO$_2$-MgO-Al$_2$O$_3$ (CSMA) system was prepared, and the structural variations and their relationship with thermophysical properties were investigated. The aforementioned four types of oxides are in fact the main compositions of a BFS.[3,4]

Generally, there are two aspects involved in understanding the relationship between the structures of molten slags and their crystallization behaviors. First, crystals are formed from liquid slags, i.e., with decreasing temperature, the crystals are precipitated gradually.

YONGQI SUN and HAO WANG are with the Department of Energy and Resources Engineering, College of Engineering, University, Beijing 100871 People's Republic of China. ZUOTAI ZHANG is with the School of Environmental Science and Engineering, South University of Science and Technology of China, Shenzhen 518055, People's Republic of China and also with Key Laboratory of Municipal Solid Waste Recycling Technology and Management of Shenzhen City, Shenzhen 518055, People's Republic of China. Contact e-mail: zhangzt@sustc.edu.cn

Thus, the crystallization behaviors of slags should be determined by the microscopic structures of the slags since the liquid state of slags is the initial state. In fact, many previous studies[10-13] investigated the crystallization behaviors of liquid slags and characterized them from the viewpoint of microscopic structures. Second, the liquid slags are formed from various equilibrium minerals, *i.e.*, with increasing temperature. The mixture of various minerals will be melted, and thus, the liquid slag is formed. Therefore, various local structural units that correspond to those in the original compositions (minerals) should remain in the liquid slags.[14]

The discussion in this study was based on the foregoing two aspects, and the relationship between microscopic structures and macroscopic properties was mainly considered. With regard to this, the microscopic structures of a CSMA system were identified using various techniques in parallel, while the macroscopic properties of slags, including viscosity and crystallization behaviors, were clarified based on both the thermodynamic calculations in this study and previous experimental tests. It should be noted that the macroscopic properties and microscopic structures comprise a pair-concept characterizing the slags, while the emphasis of the description of thermophysical properties was on the molten slags at high temperatures. The present work, thus, aims to deepen the understanding of the slag structure and their properties from a new respect.

II. MATERIALS AND METHODS

A. *Sample Preparation*

In this study, samples of a basic quaternary CSMA system were prepared with a fixed basicity of 1.05 (mass ratio of CaO to SiO$_2$) and an Al$_2$O$_3$ content range of 6 to 23 pct, as listed in Table I *via* the traditional melting-quenching method. First, pure oxides of CaO (99.9 pct), SiO$_2$ (99.8 pct), MgO (99 pct), and Al$_2$O$_3$ (99.9 pct) (Alfa Aesar Company) were weighed, thoroughly mixed and placed in a Pt crucible. The mixture was heated to 1773 K (1500 °C) and held for 2 hours under an Ar atmosphere to obtain the liquid states. Consequently, the high temperature melts were quenched to obtain the glassy samples.

The prepared glasses were then dried and ground into fewer than 200 meshes for further structural measurements. The chemical compositions of these powders were verified using the X-ray fluorescence (XRF) technique, as listed in Table I, which showed little deviation with the designed powders. Additionally, to confirm the

glassy state, these powders were characterized using the X-ray diffraction (XRD) technique, and the results displayed in Figure 1 indicated that no crystal was precipitated.

B. *Spectral Measurements*

In this study, the structures of the glassy samples were characterized using Fourier transformation infrared (FTIR), Raman and magic angular spinning nuclear magnetic resonance (MAS-NMR) spectra. First, the slags were characterized using an IR spectrophotometer (Tensor 27, Bruker, Germany) that was equipped with a KBr detector. The spectra were collected in the range of 4000 to 400 cm^{-1} with a resolution of 2 cm^{-1}, and here the IR absorption was used. Second, the Raman spectra of the samples were recorded in the range of 200 to 2000 cm^{-1} at room temperature using a JY-HR800 spectrometer (Jobin–Yvon Company, France) with a light source produced by a 1 mW semiconductor with an excitation wavelength of 532 nm.

To further clarify the structural roles of elemental Al in the glass samples directly, a solid-state ^{27}Al MAS-NMR measurement was conducted using a 400M FT-NMR spectrometer (Avance III 400M, Bruker, Germany) with an MAS probe of a 4-mm ZrO$_2$ rotor and two pairs of DuPont Vespel caps.

C. *Thermophysical Properties of the Molten Slags*

To further verify the structural analysis, the relationship between the microscopic glassy structures and macroscopic properties was clarified, which accounted for one main objective of this study. The analysis was generally conducted from two aspects. First, the present structural results in a basic CSMA quaternary system were compared with the results from related previous studies[8,9] that experimentally measured the thermophysical properties of molten slags. Second, the thermophysical properties of slags, such as viscosity and crystallization behaviors, were theoretically calculated using FactSage software herein.[15]

III. RESULTS AND DISCUSSION

A. *FTIR and Raman Spectra of the Slags*

To clarify the structures of the glasses, the prepared samples were first characterized qualitatively using FTIR, as presented in Figure 2. As can be noted, the entire FTIR spectrum could be divided into the

Table I. Chemical Compositions of the Prepared Samples by XRF (Wt Pct)

Samples	CaO (Pct)	SiO$_2$ (Pct)	MgO (Pct)	Al$_2$O$_3$ (Pct)	Basicity (CaO/SiO$_2$)
CSMA-1	43.50	41.40	9.20	6.00	1.05
CSMA-2	40.70	38.90	9.20	11.30	1.05
CSMA-3	37.50	36.70	9.20	16.60	1.02
CSMA-4	35.80	35.10	9.10	20.00	1.02
CSMA-5	34.30	33.50	9.00	23.10	1.02

following three bands: a band from 400 to 600 cm^{-1} assigned to the Si-O-Si bending vibrations, a band from 600 to 800 cm^{-1} assigned to the Si-O symmetry stretching vibrations and a band from 800 to 1200 cm^{-1} assigned to the stretching vibrations of the AlO_4 and SiO_4 tetrahedrons.[16-18] With increasing Al_2O_3 content, the intensity of the Si-O-Si bending (400 to 600 cm^{-1}) and Si-O symmetry (600 to 800 cm^{-1}) vibrations was less pronounced due to the relative decrease in the SiO_2 content in the glasses. Furthermore, it was found that the center of 800 to 1200 cm^{-1} band gradually shifted to the higher wavenumber range, which generally indicated that the degree of polymerization (DOP) of glassy networks increased; in other words, Al_2O_3 mainly acted as a network former in the present glasses.

The glasses were further characterized using the Raman spectral technique, and the results are shown in Figure 3. As can be observed, the entire Raman spectra could be divided into the following three bands: a low Raman shift range of 200 to 600 cm^{-1} generally assigned to the T-O-T bending vibrations (T represents Al or Si atoms), a medium Raman shift range of 600 to 800 cm^{-1} that originated from the Si-O symmetry

stretching vibrations and a high Raman shift range of 800 to 1100 cm^{-1} ascribed to the stretching vibrations of the AlO_4 and SiO_4 tetrahedrons,[19-21] which was consistent with the FTIR results. In particular, with varying Al_2O_3 content, the shapes and intensities of bands in the Raman spectra gradually changed.

First, in the Raman shift range of 200 to 600 cm^{-1}, the band centered at 350 cm^{-1} assigned to the Si-O-Si bending vibrations decayed with increasing Al_2O_3 content in agreement with the FTIR results, whereas the band at 550 cm^{-1} assigned to the Al-O-Al and Al-O-Si bending vibrations became more pronounced. In the silicate glasses, additional Al atoms were preferentially introduced into the central networks due to the Al avoidance effect, while the Si atoms mainly acted as boundary tetrahedral sites.[16,22,23] Thus, with increasing Al_2O_3 content, more Al atoms were inserted into the networks, and as a result, the number of bridging oxygens (BOs) between the two SiO_4 tetrahedrons decreased. Second, the intensity of the 600 to 800 cm^{-1} band decreased with increasing Al_2O_3 content, indicating that the Si-O symmetry stretching vibration weakened, which agreed with the variation trends of the 200 to 600 cm^{-1} band and the FTIR results. This could be caused by two factors: the absolute decrease in SiO_2 content and additional Si atoms behaving as boundary SiO_4 tetrahedrons with increasing Al_2O_3 content.

Third, in the high Raman shift range of 800 to 1100 cm^{-1}, the stretching vibrations of the AlO_4 and SiO_4 tetrahedrons also showed a continuous variation trend overall. The peak at ~870 cm^{-1}, generally related to the vibration of $Q^0(Si)$,[18-21] gradually diminished with increasing Al_2O_3 content, indicating fewer isolated SiO_4 tetrahedrons. The structural units related to the SiO_4 tetrahedron are conventionally denoted as $Q^i(Si)$ ($i = 0, 1, 2, 3, 4$), where i represents the number of BOs per coordinated Si atom. In addition, the shoulder at ~980 cm^{-1}, associated with the vibration of $Q^2(Si)$,[18-21] gradually decayed with increasing Al_2O_3 content, which was consistent with the decreasing Si-O-Si bending vibrations at 350 cm^{-1}. Moreover, the decreasing content of $Q^0(Si)$ and $Q^2(Si)$ in the networks also indicated less symmetry stretching vibrations of Si-O in the
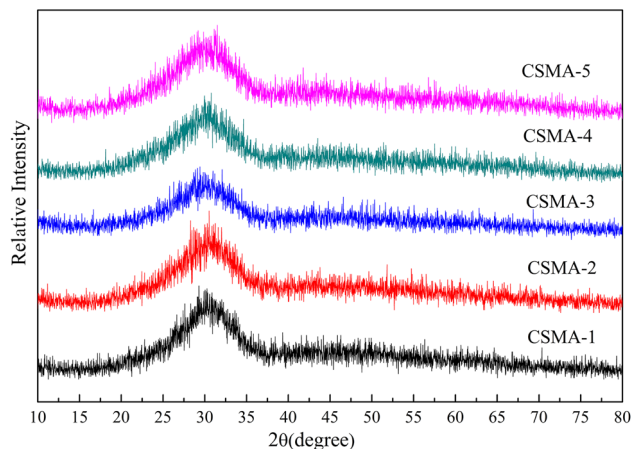

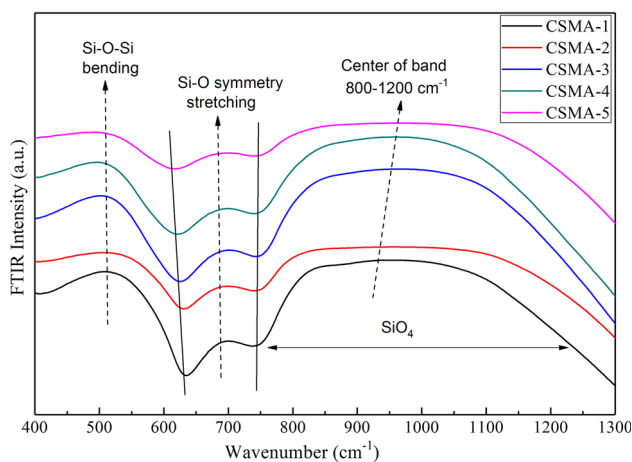Fig. 1—XRD results of the prepared glassy samples.

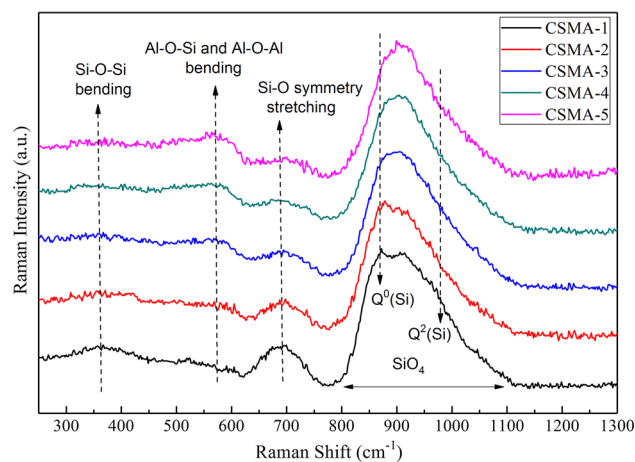Fig. 2—FTIR spectra of the prepared glassy samples.

Fig. 3—Raman spectra of the prepared glassy samples.

networks, which is in good agreement with the variation trend of 600 to 800 cm^{-1} band.

B. ^{27}Al MAS-NMR Spectra of the Molten Slags

The FTIR and Raman spectra mainly identified the structural variations in SiO_2 in the networks; as a main variable, the structural variations of Al_2O_3 can be understood directly. Thus, the ^{27}Al MAS-NMR spectra were collected, and the results are shown in Figure 4. As can be observed from Figure 4(a), the NMR spectra were mainly located in the chemical shift range of -20 to 100 ppm and did not present a symmetric shape. In detail, there was a dominant peak at ~55 ppm, which was generally assigned to the stretching vibrations of the AlO_4 tetrahedron, while a small shoulder existed at ~25 ppm, which was assigned to AlO_5 and AlO_6,[22,24,25] acting as charge compensators of the AlO_4 tetrahedron. This result proved that Al_2O_3 was a typical amphoteric oxide that mainly acted as a network former in the present glasses, which agrees with the foregoing FTIR and Raman results.

With regard to the effect of the Al_2O_3 content, Figure 4(a) displays that the overall shape and relative intensity of various bands did not change remarkably with varying Al_2O_3 content. This finding indicated that in all samples, Al_2O_3 mainly acted as a network former, and the relative contents of AlO_4, AlO_5, and AlO_6 did not prominently vary. Furthermore, by enlarging the NMR spectra, their characteristics could be analyzed more accurately, as presented in Figure 4(b). It can be seen that the width of the effective NMR envelope of -20 to 100 ppm slightly and continuously increased with increasing Al_2O_3 content. From the viewpoint of spectral deconvolution, a wide NMR envelop could suggest a broader distribution of the Al-related structural units. In other words, this broad distribution could qualitatively suggest an increasing content of AlO_5 and AlO_6 with increasing Al_2O_3 content. Although in all samples, Al_2O_3 dominantly acted as a network former, and its role of a network modifier was continuously enhanced with increasing Al_2O_3 content; however, the effect was relatively weak.

C. Spectral Fittings and the Structural Analysis

To further identify the silicate structure quantitatively, the high Raman shift range of 800 to 1100 cm^{-1} in the Raman spectra could be fitted using four Gaussian functions assigned to the four $Q^i(Si)$ units, namely, $Q^0(Si)$, $Q^1(Si)$, $Q^2(Si)$, and $Q^3(Si)$, which are generally located at ~870, ~960, ~990, and ~1050 cm^{-1}, respectively.[18–21,26,27] The fitting results of various Raman curves are presented in Figure 5, and these four Gaussian functions are well fitted by the Raman curve, indicating the reasonableness of the present methodology.

Based on the areas of obtained peaks (A_i) and the Raman scattering coefficient (S_i) of $Q^i(Si)$, the mole fractions (X_i) ($i = 0, 1, 2, 3$) of various $Q^i(Si)$ could be calculated by means of Eq. [1]:

$$X_i = (A_i/S_i)/\left(\sum_{i=0}^{3} A_i/S_i\right), \qquad [1]$$

where the values of S_0, S_1, S_2, and S_3 are 1, 0.514, 0.242, and 0.09, respectively.[28,29]

The results are shown in Figure 6, and as can be observed, with increasing Al_2O_3 content, the concentrations of $Q^0(Si)$ and $Q^2(Si)$ decreased, while those of $Q^1(Si)$ and $Q^3(Si)$ increased, in qualitative agreement with the FTIR and Raman results. These results suggested that the mole ratio of the symmetric SiO_4 tetrahedron decreased with increasing Al_2O_3 addition. In other words, Al atoms were preferentially introduced into the central sites of networks to form the AlO_4 tetrahedron, and as a result, more Si atoms formed boundary SiO_4 tetrahedrons such as $Q^1(Si)$ and $Q^3(Si)$.

Additionally, based on the concentrations of various $Q^i(Si)$, the average number of BOs per coordinated Si atom could be calculated using Eq. [2], which were 2.09, 2.12, 2.16, 2.18, and 2.29 for samples CSMA-1, CSMA-2, CSMA-3, CSMA-4, and CSMA-5, respectively. This finding demonstrated quantitatively that an increasing Al_2O_3 content continuously increased the BO contents. In addition to the increasing BO numbers in the Al-O-Si units, the DOP of the slags was thus increased pronouncedly. In other words, Al_2O_3 mainly acted as a network former.

$$\bar{i} = \sum_i iX_i. \qquad [2]$$

Additionally, based on the average BO numbers per coordinated Si atom, the average number of bound oxygen atoms per coordinated Si atom could be calculated using Eq. [3]. Meanwhile, the initial numbers of bound oxygen atoms per coordinated Si without Al_2O_3 could be calculated using Eq. [4]. The results are shown in Figure 7, based on which several characteristics could be obtained. First, in the absence of Al_2O_3, the number of bound oxygen atoms per Si increased from sample CSMA-1 to CSMA-5 due to the increasing relative content of MgO. Second, in the presence of Al_2O_3, the number of bound oxygen atoms per Si decreased greatly, which indicated that the structural networks were polymerized remarkably. Thus, a higher slag DOP was induced. Third, with increasing Al_2O_3 content, the number of bound oxygen atoms per Si continuously increased because the added Al-O-Al bond incorporated the non-BO (NBO) from the Si-NBO units, as described by Eqs. [5] and [6]. As a result, a more polymerized structure was induced by Al_2O_3.

$$\bar{O} = \frac{1}{2}BO + (4 - BO), \qquad [3]$$

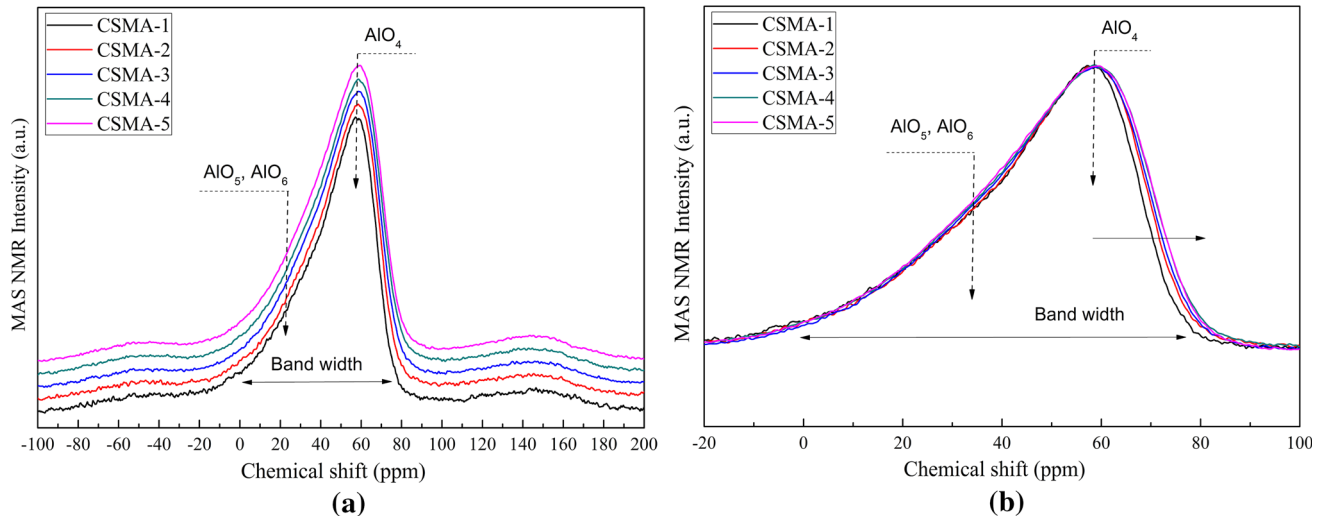$$\bar{O} = \frac{w_{CaO}/56 + 2w_{SiO_2}/60 + w_{MgO}/40}{w_{SiO_2}/60}, \qquad [4]$$

Fig. 4—MAS-NMR spectra of the glasses, (*a*) NMR spectra and (*b*) change in the band width with varying Al_2O_3 contents.

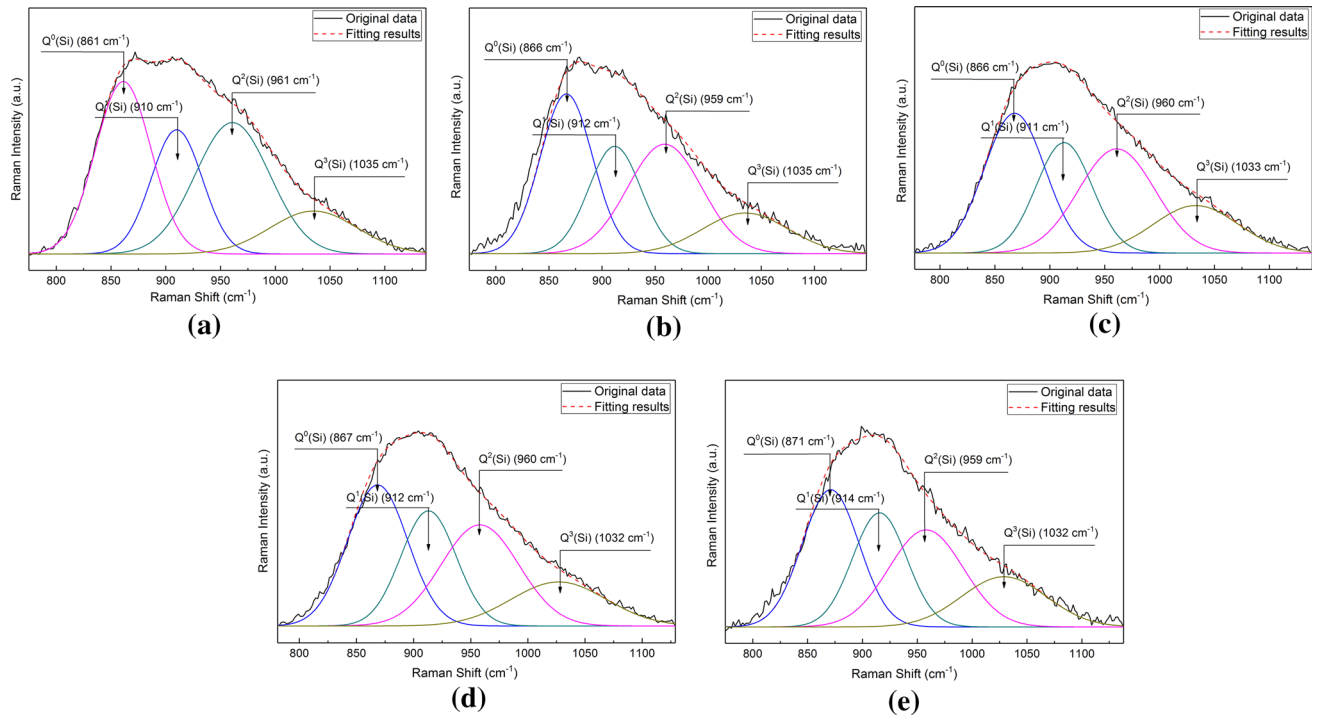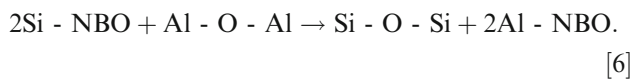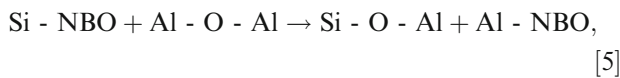Fig. 5—Fitting processes of the Raman spectra of (*a*) CSMA-1, (*b*) CSMA-2, (*c*) CSMA-3, (*d*) CSMA-4, and (*e*) CSMA-5.

$$Si - NBO + Al - O - Al \rightarrow Si - O - Al + Al - NBO, \quad [5]$$

$$2Si - NBO + Al - O - Al \rightarrow Si - O - Si + 2Al - NBO. \quad [6]$$

Similarly, to quantify the mole ratios of various Al-related structural units, the ^{27}Al MAS-NMR spectra obtained could be fitted using three Gaussian functions associated with AlO_4, AlO_5, and AlO_6 located at ~60, ~35, and ~8 ppm, respectively.[22,24,25] The fitting results are shown in Figure 8, and it can be observed that compared to the qualitative analysis, the quantitative results demonstrated that there were high contents of AlO_5 and AlO_6 in the networks, which acted as charge compensators of AlO_4 in addition to Ca^{2+} and Mg^{2+}.

Furthermore, based on the areas of the obtained peaks, the mole fractions of various Al-related structural units could be calculated by Eq. [7]. The results shown in Figure 9 indicated high contents of both AlO_4 and AlO_5 in the networks, proving the amphoteric effect of Al_2O_3. Furthermore, with increasing Al_2O_3 content, the
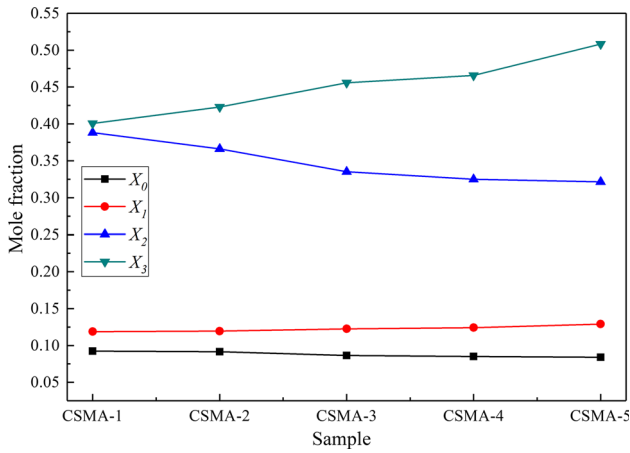
Fig. 6—Concentrations of various $Q^i(Si)$ units based on Raman fittings.
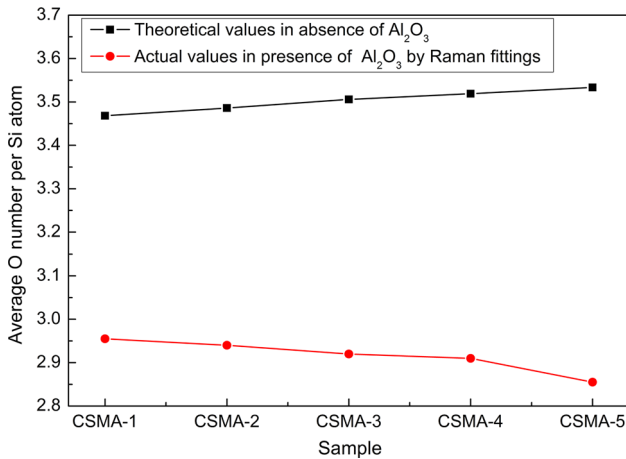

Fig. 7—Number of bound oxygen atoms per coordinated Si atom.

mole ratios of AlO_5 and AlO_6 increased continuously from 43 and 7.0 to 48 and 7.4 pct, respectively, while that of AlO_4 decreased gradually, indicating the improved basicity of Al_2O_3 in the networks. This finding is also in agreement with the qualitative variation that the band width of NMR spectra slightly increased with increasing Al_2O_3 content.

$$X_{AlO_i} = A_{AlO_i} \Big/ \left(\sum_{i=4}^{3} A_{AlO_i} \right). \quad [7]$$

To overall estimate the role of Al_2O_3 in the networks, another respect could be considered, i.e., to compare the mole ratios of AlO_4, AlO_5, and AlO_6 in the present system with those in the pure Al_2O_3 liquids, since in a pure Al_2O_3 melt, Al_2O_3 can act as both a network former of AlO_4 and network modifiers of AlO_5 and AlO_6. According to a previous theoretical calculation[30] in pure Al_2O_3 liquids at 3000 K (2727 °C), the concentrations of AlO_4, AlO_5, and AlO_6 were 24, 58, and 18 pct, respectively, while in the presence of the CSMA

system, the concentrations of AlO_4, AlO_5, and AlO_6 were approximately 48, 45, and 7 pct, respectively. Accordingly, the concentration of AlO_4 in the present system was higher than that in pure Al_2O_3 melt, whereas the concentrations of AlO_5 and AlO_6 in the present system were lower. This undoubtedly proved that in the present system, although AlO_4, AlO_5, and AlO_6 coexisted in the slags, Al_2O_3 acted as a network former overall. As a result, the DOP of the slags increased with increasing Al_2O_3 content.

D. Relationship Between Microscopic Structures and Crystallization Behavior of the Slags

1. Viscous flow of the molten slags

To relate the microscopic structures to the macroscopic properties of the molten slags, the viscosity of the CSMA system was first calculated in the temperature range of 1473 K to 1973 K (1200 °C to 1650 °C) herein. The results are displayed in Figure 10. As can been seen, at high temperatures where only liquid slags exist, the viscosity of the slags continuously increased with increasing Al_2O_3 content in the range of 6 to 23 pct. This finding proved that in the present system, Al_2O_3 acted as an acidic oxide, viz., a network former in all samples, which is consistent with the foregoing structural analysis that an increasing DOP of the networks was continuously caused by Al_2O_3. However, at low temperatures, the slag viscosity cannot be directly related to the slag microstructure due to the formation of solid minerals, although in this case, the variation in the slag viscosity did not change with varying Al_2O_3 contents.

Furthermore, the microscopic structures of slags identified herein could be understood in a greater context from the viewpoint of viscous flows. Table II summarizes the viscosities of various Al_2O_3 bearing slags from previous studies,[16,23,33-48] including the simple CSA system (CaO-SiO_2-Al_2O_3, Group I), the CSA system with other components (Group II), the complex CSMA system (Group III) system, and the CSMA system with other components (Group IV).

In most cases, the viscosities of the slags increased with increasing Al_2O_3 content, especially when the Al_2O_3 content was relatively low.[23,31,33-37,41-48] This indicated that, in general, Al_2O_3 acted as an acidic oxide, which agrees with the present results. However, according to the structural analysis here, the amphoteric effect of Al_2O_3 always existed, although sometimes it was not directly reflected. Looking at this from a different viewpoint, it is shown in Table II that in several Al_2O_3-bearing slags,[16,32,39,40] the viscosities first increased and then decreased with increasing Al_2O_3 content. This trend mainly appeared in two cases: with high Al_2O_3 content and with sufficient network formers such as SiO_2 in the slags. These results illustrated the amphoteric effect of Al_2O_3, and in fact directly demonstrated the structural analysis herein, i.e., the acidity of Al_2O_3 in the networks decreased, whereas basicity of Al_2O_3 increased with increasing Al_2O_3 content despite the varying chemical compositions of the slags.
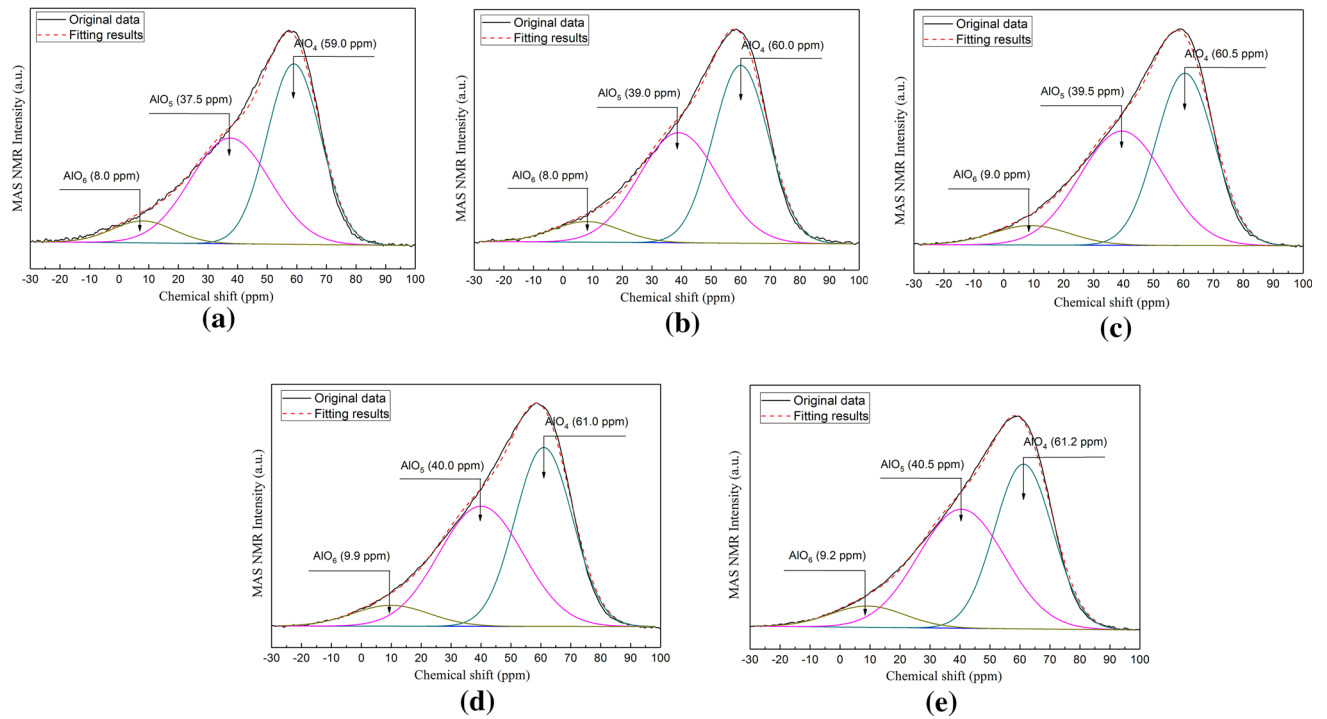
Fig. 8—Fitting processes of the ^{27}Al MAS-NMR spectra of (*a*) CSMA-1, (*b*) CSMA-2, (*c*) CSMA-3, (*d*) CSMA-4, and (*e*) CSMA-5.
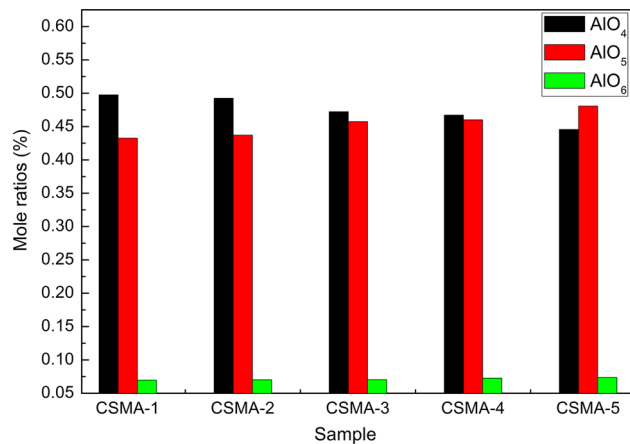

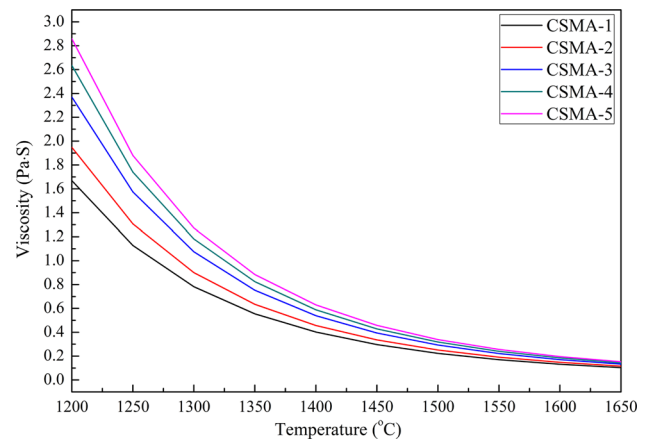Fig. 9—Concentrations of various Al-related structural units based on NMR fittings.

Fig. 10—Viscosities of the present molten slags.

2. *Crystallization behaviors of the molten slags*

To further verify the microscopic structural analysis, the crystallization behaviors of molten slags were then analyzed herein. First, the isopleth phase diagrams of these samples were calculated, as shown in Figures 11(a) through (e). As can be seen with decreasing temperature, a series of crystals are precipitated stepwise in the liquid slags. Finally, the liquid phase disappears. The main mineral phases in the solid slags were melilite, spinel, and other phases. Generally, the first crystalline phase precipitated was defined as the primary phase, and the temperature where it was formed was defined as the crystallization temperature. The primary phase and crystallization temperature are two key parameters that

reflect the crystallization ability of the slags, which are mainly discussed here.

Summarizing the main information on crystallization behaviors in Figure 11, the primary phase and the corresponding crystallization temperature was obtained, as shown in Figure 12. As can be observed, first with increasing Al_2O_3 content, the primary phase changed from $Ca_3MgSi_2O_8$ in CSMA-1, and melilite in CSMA-2, CSMA-3, and CSMA-4 to $MgAlO_4$ in CSMA-5. For the melilite phase, its special molecular composition changed from $Ca_2MgSi_2O_7$ (akermanite) to $Ca_2Al_2SiO_7$ (gehlenite) with increasing Al_2O_3 content from 11 to 20 pct, as experimentally demonstrated by the previous studies.[8,9,49] Furthermore, with increasing Al_2O_3 content, the crystallization temperature first increased and then decreased. This proved that, in the present system,

Table II. Viscosities of Al₂O₃-Bearing Melts from Previous Studies Obtained by Experimental Measurements

| Slag Systems	Basicity (B)	Al$_2$O$_3$ (Wt Pct)	Other Components	Temperature Range (K)	Viscosity (Increasing Al$_2$O$_3$ Content)	References
Group I (CSA) (CaO-SiO$_2$-Al$_2$O$_3$)	0.14 to 1.29	0 to 35		1423 to 1773	increased	31
	0.58 to 1.17	5 to 30		1714 to 1818	first increased and then decreased	32
	1.00, 1.30	0 to 20		1600 to 1823	first increased and then decreased	16
Group II (CSA + Other Components)	1.07 to 5.69	10 to 29	Na$_2$O, Li$_2$O	1548 to 1773	increased	33
	1.01 to 9.22	9 to 30	Na$_2$O, CaF$_2$	1523 to 1773	increased	34
	0.82	0 to 13	FeO, CaF$_2$	1714 to 1757	increased	35
	0.64	0 to 10	K$_2$O	1663 to 1813	increased	36
	1.00	12 to 18	TiO$_2$, Fe$_2$O$_3$	1573 to 1873	increased	37
Group III (CSMA) (CaO-SiO$_2$-MgO-Al$_2$O$_3$)	0.59 to 0.97	5.5 to 25		1748 to 1873	decreased	38
	1.00	16 to 19		1573 to 1873	increased	37
	1.00	14 to 17		1653 to 1773	first increased and then decreased	39
	1.00, 1.30	10 to 20		1600 to 1823	first increased and then decreased	16
	0.50 to 0.90	5 to 20		1540 to 1798	first increased and then decreased	40
	0.08 to 0.66	0 to 25		1623 to 1773	increased	41
	0.10 to 1.29	15 to 35		1573 to 1773	increased	42,43
	0.80 to 1.30	0 to 20		1623 to 1773	increased	44
Group IV (CSMA + Other Components)	0.13 to 0.16	1 to 14	Na$_2$O	1343 to 1773	increased	45
	0.22 to 0.91	5 to 40	Na$_2$O, Li$_2$O, MnO, CaF$_2$	1473 to 1673	increased	46
	1.18 to 1.45	10 to 18	FeO	1613 to 1773	increased	47
	1.26	0 to 25	FeO	1513 to 1823	increased	48
	2.38 to 10.40	24 to 35	CaF$_2$	1773 to 1873	increased	23
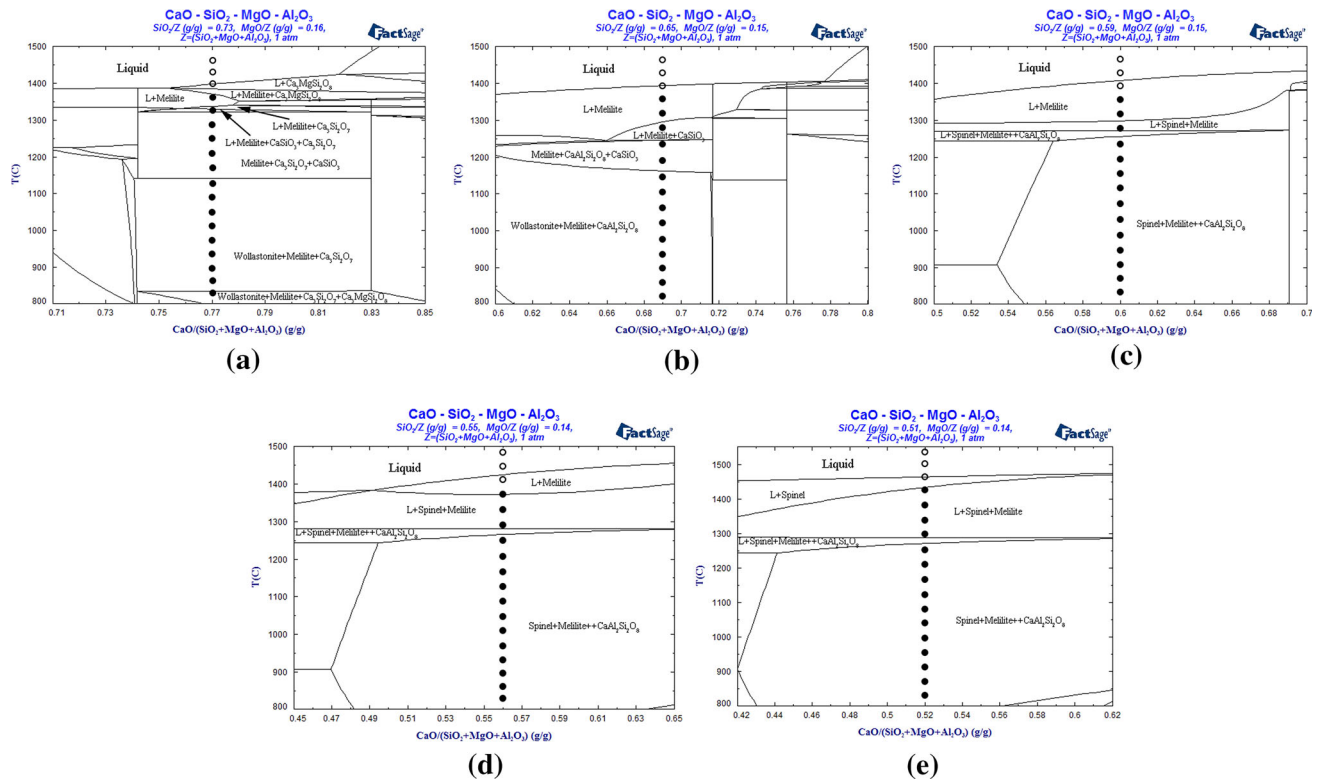
Fig. 11—Isopleth phase diagrams for samples (a) CSMA-1, (b) CSMA-2, (c) CSMA-3, (d) CSMA-4, and (e) CSMA-5.
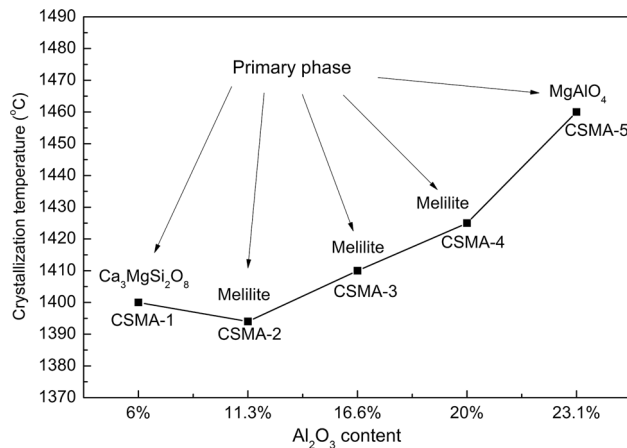

Fig. 12—Primary phase and its crystallization temperature of the molten slags.

from the viewpoint of the equilibrium crystallization temperature of the primary phase, the crystallization ability of the slags first decreased and then increased with increasing Al_2O_3 content, which agrees with our previous experimental results,[8,9] as evidenced by the critical cooling rates from the kinetics.

Furthermore, the crystallization behaviors of the slags could be correlated with the microscopic structural changes. For the primary phase of $Ca_2MgSi_2O_7$ in the slags with a low Al_2O_3 content, its main structural framework was O-Si-O-Ca-O-Si-O-Mg, where Ca^{2+} acted as charge balance, which could be rewritten as Si-NBO-Ca-NBO-Si based on the structural units in the

molten slags. With increasing Al_2O_3 content, the DOP of the networks increased, and thus the concentrations of the NBO-Si units decreased. Therefore, the number of Ca-NBO-Si groups decreased in the networks, and the number of Si-NBO-Ca-NBO-Si frames decreased; as a result, the precipitation of $Ca_2MgSi_2O_7$ was inhibited with a higher Al_2O_3 content. On the other hand, with increasing Al_2O_3 content, the mole ratios of $Q^0(Si)$ and $Q^2(Si)$ decreased, while those of $Q^1(Si)$ and $Q^3(Si)$ increased. This means that the contents of the symmetric SiO_4 units in the networks decreased, which could also inhibit the precipitation of $Ca_2MgSi_2O_7$ from the viewpoint of structural ordering, since generally the structures of crystals are more ordered both locally and at a long range.[50,51]

With further increasing Al_2O_3 content, the number of Ca-NBO-Si groups continuously decreased, and finally the primary phase changed from $Ca_2MgSi_2O_7$ to $Ca_2Al_2SiO_7$. For the primary phase of $Ca_2Al_2SiO_7$ in slags with a high Al_2O_3 content, its main structural framework was O-Si-O-Ca-O-Al-O-Ca, rewritten as Si-NBO-Ca-NBO-Al. With increasing Al_2O_3 content, the number of Ca-NBO-Al groups in the networks increased, and thus the precipitation of $Ca_2Al_2SiO_7$ was improved. In addition, based on the NMR results, the number of AlO_6 groups in the networks also increased with increasing Al_2O_3 content and actually behaved as a framework unit in $Ca_2Al_2SiO_7$. As a result, the precipitation of $Ca_2Al_2SiO_7$ increased with increasing Al_2O_3 content, and finally a higher crystallization temperature or higher crystallization ability ensued.

In particular, as the sample changed from CSMA-1 to CSMA-2, the primary phase was transformed from $Ca_3MgSi_2O_8$ to $Ca_2MgSi_2O_7$, while their crystallization temperature decreased. The main structural units of $Ca_3MgSi_2O_8$ were Ca-NBO-Si and Mg-NBO-Si groups, which was similar to those of $Ca_2MgSi_2O_7$. With increasing Al_2O_3 content, the DOP of the slags increased, and meanwhile the numbers of Ca-NBO-Si units decreased in the networks. This effect could cause two results, *i.e.*, a decrease in the Ca-NBO numbers and an increase in the BO numbers in the primary phases. As a result, $Ca_3MgSi_2O_8$ that precipitated from the liquid slags was replaced by $Ca_2MgSi_2O_7$. With regard to the crystallization temperature and due to the similar structural units of $Ca_3MgSi_2O_8$ and $Ca_2MgSi_2O_7$, a competitive effect existed between these two phases, *i.e.*, either phase can be precipitated as the primary phase. In other words, the potential precipitation of $Ca_2MgSi_2O_7$ could resist the formation of $Ca_3MgSi_2O_8$. As a result, the crystallization temperature decreased from CSMA-1 to CSMA-2, *i.e.*, the crystallization ability of the slags decreased.

Furthermore, it is shown in Figures 11 and 12 that the spinel of $MgAlO_4$ accounted for a significant crystalline phase formed in the slags, which became the primary crystalline phase with an increase in Al_2O_3 content to 23 pct. In the structures of $MgAlO_4$, an Al atom was coordinated with six oxygen atoms, acting as an AlO_6 octahedron. According to the structural analysis of slags, an increasing Al_2O_3 content increased the content of AlO_6 octahedrons in the networks, which enhanced the precipitation of $MgAlO_4$ in the slags. In addition, finally, $MgAlO_4$ became the primary phase preferentially formed from the liquid slags.

IV. CONCLUSIONS

In this study, the relationship between the structures and the thermophysical properties of CSMA molten slags was identified using FTIR, Raman, and ^{27}Al MAS-NMR techniques. The FTIR spectra qualitatively and the Raman fittings quantitatively proved that the DOP of the networks increased with increasing Al_2O_3 content, resulting in an increasing viscosity of the slags. The fittings of ^{27}Al MAS-NMR spectra proved that AlO_4, AlO_5, and AlO_6 coexist in the networks, and the concentrations of AlO_5 and AlO_6 increased with increasing Al_2O_3 content. The specific changes in the slag microscopic structures induced the change in the primary phase precipitated in the slags from $Ca_2MgSi_2O_7$ and $Ca_2Al_2SiO_7$ to $MgAlO_4$. Correspondingly, their crystallization temperatures first decreased and then increased with a transition point at ~15 wt pct Al_2O_3.

REFERENCES

1. X. Ma, D. Zhang, Z. Zhao, T. Evans, and B. Zhao: *ISIJ Int.*, 2016, vol. 56, pp. 513–19.
2. M. Matsumura, M. Hoshi, and T. Kawaguchi: *ISIJ Int.*, 2005, vol. 45, pp. 594–602.
3. H. Zhang, H. Wang, X. Zhu, Y.J. Qiu, K. Li, R. Chen, and Q. Liao: *Appl. Energy*, 2013, vol. 112, pp. 956–66.
4. M. Barati, S. Esfahani, and T.A. Utigard: *Energy*, 2011, vol. 36, pp. 5440–49.
5. Y. Sun, Z. Zhang, L. Liu, and X. Wang: *Energies*, 2015, vol. 8, pp. 1917–35.
6. T. Mizuochi, T. Akiyama, T. Shimada, E. Kasai, and J.I. Yagi: *ISIJ Int.*, 2001, vol. 41, pp. 1423–28.
7. H. Purwanto, T. Mizuochi, and T. Akiyama: *Mater. Trans.*, 2005, vol. 46, pp. 1324–30.
8. Y. Sun, H. Shen, H. Wang, X. Wang, and Z. Zhang: *Energy*, 2014, vol. 76, pp. 761–67.
9. Y. Sun, Z. Zhang, L. Liu, and X. Wang: *Energies*, 2014, vol. 7, pp. 1673–84.
10. Y. Sun, Z. Zhang, L. Liu, and X. Wang: *J. Noncryst. Solids*, 2015, vol. 420, pp. 26–33.
11. Z. Wang, Y. Sun, S. Sridhar, M. Zhang, M. Guo, and Z. Zhang: *Metall. Mater. Trans. B*, 2015, vol. 46B, pp. 2246–54.
12. Z. Li, J. Li, Y. Sun, S. Seetharaman, L. Liu, X. Wang, and Z. Zhang: *Metall. Mater. Trans. B*, 2016, vol. 47B, pp. 1390–99.
13. S.S. Jung and I. Sohn: *Environ. Sci. Technol.*, 2014, vol. 48, pp. 1886–92.
14. Z. Wu, M. Li, W. Wang, and K. Liu: *Nat. Commun.*, 2015, https://doi.org/10.1038/ncomms7035.
15. C.W. Bale, E. Bélisle, P. Chartrand, S.A. Decterov, G. Eriksson, K. Hack, I.H. Jung, Y.B. Kang, J. Melançon, A.D. Pelton, C. Robelin, and S. Petersen: *Calphad*, 2009, vol. 33, pp. 295–311.
16. J.H. Park, D.J. Min, and H.S. Song: *Metall. Mater. Trans. B*, 2004, vol. 35B, pp. 269–75.
17. J.H. Park, D.J. Min, and H.S. Song: *ISIJ Int.*, 2002, vol. 42, pp. 344–51.
18. J. Li, Y. Sun, Z. Li, Z. Zhang *et al.*: *ISIJ Int.*, 2016, vol. 56, pp. 752–58.
19. D.R. Neuville, D. de Ligny, and G.S. Henderson: *Rev. Mineral. Geochem.*, 2014, vol. 78, pp. 509–41.
20. L.G. Hwa, S.L. Hwang, and L.C. Liu: *J. Noncryst. Solids*, 1998, vol. 238, pp. 193–97.
21. I. Daniel, P. Gillet, B.T. Poe, and P.F. McMillan: *Phys. Chem. Miner.*, 1995, vol. 22, pp. 74–86.
22. D.R. Neuville, L. Cormier, V. Montouillout, P. Florian, F. Millot, J.C. Rifflet, and D. Massiot: *Am. Mineral.*, 2008, vol. 93, pp. 1721–31.
23. T.S. Kim and J.H. Park: *ISIJ Int.*, 2014, vol. 54, pp. 2031–38.
24. D.R. Neuville, L. Cormier, and D. Massiot: *Chem. Geol.*, 2006, vol. 229, pp. 173–85.
25. D.R. Neuville, L. Cormier, and D. Massiot: *Geochim. Cosmochim. Acta*, 2004, vol. 68, pp. 5071–79.
26. B.O. Mysen: *Am. Mineral.*, 1996, vol. 81, pp. 1531–34.
27. P.F. McMillan: *Am. Mineral.*, 1984, vol. 69, pp. 622–44.
28. J.D. Frantza and B.O. Mysen: *Chem. Geol.*, 1995, vol. 121, pp. 155–76.
29. Y. Wu, G. Jiang, J. You, H. Hou, and H. Chen: *Acta Phys. Sin.*, 2005, vol. 54, pp. 961–66.
30. B.T. Poe, P.F. McMillan, B. Cote, D. Massiot, and J.P. Coutures: *J. Am. Ceram. Soc.*, 1994, vol. 77, pp. 1832–38.
31. J.S. Machin and T.B. Yee: *J. Am. Ceram. Soc.*, 1948, vol. 31, pp. 200–04.
32. G. Zhang and K.C. Chou: *ISIJ Int.*, 2013, vol. 53, pp. 177–80.

33. G.H. Kim, C.S. Kim, and I.L. Sohn: *ISIJ Int.*, 2013, vol. 53, pp. 170–76.
34. G.H. Kim and I.L. Sohn: *J. Noncryst. Solids*, 2012, vol. 358, pp. 1530–37.
35. F. Shahbazian, S. Du, and S. Seetharaman: *ISIJ Int.*, 2002, vol. 42, pp. 155–62.
36. G. Zhang and K.C. Chou: *Metall. Mater. Trans. B*, 2012, vol. 43B, pp. 841–48.
37. N. Saito, N. Hori, K. Nakashima, and K. Mori: *Metall. Mater. Trans. B*, 2003, vol. 34B, pp. 509–16.
38. J. Liao, Y. Zhang, S. Sridhar, X. Wang, and Z. Zhang: *ISIJ Int.*, 2012, vol. 52, pp. 753–58.
39. C. Sun, X. Liu, J. Li, X. Yin, S. Song, and Q. Wang: *ISIJ Int.*, 2017, vol. 57, pp. 578–82.
40. X. Tang, Z. Zhang, M. Guo, M. Zhang, and X. Wang: *J. Iron. Steel Res. Int.*, 2011, vol. 18, pp. 1–17.
41. J.S. Machin and T.B. Yee: *J. Am. Ceram. Soc.*, 1954, vol. 37, pp. 177–86.
42. J.S. Machin, T.B. Yee, and D.L. Hanna: *J. Am. Ceram. Soc.*, 1952, vol. 35, pp. 322–25.
43. J.S. Machin and D.L. Hanna: *J. Am. Ceram. Soc.*, 1945, vol. 28, pp. 310–16.
44. H. Kim, H. Matsuura, F. Tsukihashi, W. Wang, D.J. Min, and I.L. Sohn: *Metall. Mater. Trans. B*, 2013, vol. 44B, pp. 5–12.
45. J. Cheng, Z. Xiao, K. Yang, and H. Wu: *Ceram. Int.*, 2013, vol. 39, pp. 4055–62.
46. Z. Zhang, G. Wen, P. Tang, and S. Sridhar: *ISIJ Int.*, 2008, vol. 48, pp. 739–46.
47. J.R. Kim, Y.S. Lee, D.J. Min, S.M. Jung, and S.H. Yi: *ISIJ Int.*, 2004, vol. 44, pp. 1291–97.
48. Z. Wang, Y. Sun, S. Sridhar, M. Zhang, M. Guo, and Z. Zhang: *Metall. Mater. Trans. B*, 2015, vol. 46B, pp. 537–41.
49. H. Wang, B. Ding, X. Zhu, Y. Tan, X. He, and Q. Liao: *Int. J. Heat Mass Transf.*, 2017, vol. 113, pp. 286–94.
50. S.R. Elliott: *Nature*, 1991, vol. 354, pp. 445–52.
51. P.W. Anderson: *Science*, 1995, vol. 267, pp. 1609–10.